Preprints of the 19th World Congress
The International Federation of Automatic Control
Cape Town, South Africa. August 24-29, 2014

Trajectory Planning For a Deep Drawing Tool

Timo Böhm [*], **Thomas Meurer** [**]

[*] *Group Tool Shops, Volkswagen AG, 38436 Wolfsburg, Germany (e-mail: timo.boehm@volkswagen.de).*
[**] *Chair of Automatic Control, Christian-Albrechts-University Kiel, 24143 Kiel, Germany (e-mail: tm@tf.uni-kiel.de).*

Abstract: Model-based trajectory planning is addressed for the realization of desired temperature trajectories for a deep drawing tool. Based on the distributed-parameter system description of the tool a finite element approximation is deduced which serves as basis for a systematic flatness-based design of a feedforward control. Trajectory assignment is considered by taking into account the minimization of a process-related objective function. Simulation and experimental data obtained from a fully equipped forming tool are presented for pure feedforward control and a two-degree-of-freedom control concept amending the feedforward part by an output error feedback controller. These confirm the applicability of the design technique and the tracking performance.

Keywords: deep drawing, distributed-parameter systems, trajectory planning, flatness, temperature control, experiments.

1. INTRODUCTION

The production of car bodies is a challenging field for control engineering due to the demand for zero failure production at increased shape complexity, quality standards and high throughput volumes. One essential production step is deep drawing during which a metal sheet is drawn into a die by a punch to achieve the forming process. This process is significantly influenced by a great number of varying process and material parameters. Moreover, requirements on shape sharpness and quality reduce the production window such that even small deviations from the design state may lead to scrap.

The process-related temperature is a well-known influence value depending primarily on the tribology system between the tool and the sheet, the plasticity of the sheet material and the thermoelastic properties of the tool. Typically, the temperature increases during the production process caused by friction and plastic deformation of the metal sheet, until an equilibrium is reached. Hence, during interruptions of production the tool cools down. Every deep drawing process is unique because of the shape, the tool stiffness and the blank geometry. Until now the complexity of the temperature influence and the interactions significantly complicate the development of an appropriate process simulation model. This presently prevents a reliable forecast of the temperature evolution and the interaction between the different influence and exchange factors. However, experience shows that a deviation of more than $\pm 10\,\mathrm{K}$ of the tool temperature from the operating point may already lead to defects. Experiments show that if temperature related defects are detected in the press shop, appropriate tool heating before production start improves production quality. For further information of the temperature effect on the deep drawing process, see [Böhm et al., 2013] and the references therein.

In order to realize suitable tool heating, experiments at the press shop with a tool equipped with heating cartridges showed that standard industrialized PI or PID control units are incapable of achieving the desired performance and accuracy in a fixed time span. Thereby additional constraints are imposed by a rather narrow realization window for the desired temperature set point change and the required temperature accuracy since excessively high or low tool temperatures at the production start can deteriorate the process [Böhm et al., 2013]. Hence, a sophisticated trajectory planning and control strategy is needed that takes into account the geometric extension of the tool and the resulting spatial-temporal temperature evolution in order to realize desired temperature profiles in selected areas of the tool within a fixed time span.

Trajectory planning refers to the design of a (feedforward) control such that the controlled variables of the system follow prescribed desired (spatial-temporal) reference trajectories. Given finite-dimensional nonlinear systems trajectory planning can be systematically approached exploiting differential flatness [Fliess et al., 1995]. Since the underlying idea, i.e. the existence of a one-to-one correspondence between trajectories of systems can be adapted to distributed-parameter systems (DPSs), various approaches have been suggested with a major focus on boundary actuation and DPSs in a single spatial variable, see, e.g., Fliess et al. [1997], Laroche et al. [2000], Petit and Rouchon [2001], Lynch and Rudolph [2002], Meurer and Zeitz [2005] and the references therein. Extensions to higher-dimensional spatial domains are, e.g., provided in Rudolph [2003], Petit and Rouchon [2002], Rouchon [2005], Meurer and Kugi [2009], Meurer [2011].

To address the complex shaped spatial domain of the considered deep drawing tool (cf. Fig. 1) as well as in-domain actuation by means of heating cartridges subsequently

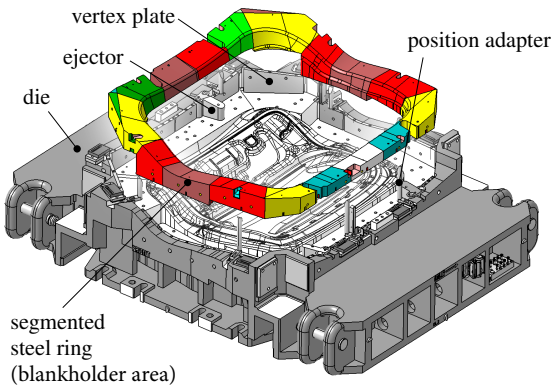

Fig. 1. Base part of the deep drawing tool (exploded view).

the flatness-based spectral design technique introduced in Meurer [2011] and further generalized in Meurer [2013] is considered and combined with output error feedback control. The underlying idea is based on the systematic construction of flat output by exploiting the properties of the spectral decomposition of so-called Riesz spectral operators (see, e.g., Curtain and Zwart [1995]). Their eigenvalues are isolated and the set of corresponding eigenvectors and adjoint eigenvectors form an orthonormal Riesz basis.

In this contribution, the spectral approach is combined with a finite element approximation of the partial differential equation (PDE) describing the spatial-temporal temperature evolution in the deep drawing tool with embedded heating cartridges. Based on the finite-dimensional representation an efficient semi-numeric trajectory planning approach is developed taking into account optimal trajectory assignment for the flat output in view of actuator constraints. Simulation and experimental results for both flatness-based feedforward control and its combination with output error feedback control are presented which illustrate the achievable tracking performance for the deep drawing tool. To the best knowledge of the authors, this presents the first implementation and experimental validation of flatness-based trajectory planning for thermal DPSs with 3-dimensional spatial domain.

2. PROBLEM FORMULATION

A deep drawing tool basically consists of the three parts, namely the blankholder, die and punch. This paper only considers the die. Fig. 1 shows the base part of the deep drawing tool of a inner backdoor with a weight of about 11.5 tons.

2.1 Continuous distributed-parameter setting

Assuming linear conditions, the spatial-temporal evolution of the (relative) temperature $x(z,t)$ in the die with 3-dimensional domain Ω is determined by the heat equation

$$\rho c_p \partial_t x = \nabla \cdot (\kappa \nabla x) + \textstyle\sum_{j=1}^{m} b_j u_j, \tag{1}$$

with $(z,t) \in \Omega \times \mathbb{R}^+$. Here, $x(z,t) = \vartheta(z,t) - \vartheta_u$, where $\vartheta(z,t)$ describes the temperature distribution in the die and ϑ_u is the ambient temperature, assumed to be constant and uniform. The terms $\rho(z)$, $c_p(z)$ and $\kappa(z)$ refer to density, specific heat capacity and thermal conductivity. The coefficient $b_j(z)$ represents the j-th spatial actuator characteristics with $u_j(t)$ denoting the power of the heating cartridges. Since only heating but not cooling is possible, constraints

$$u_j(t) \in [0, \bar{u}], \quad j = 1, \ldots, m \tag{2}$$

apply. Dirichlet and Robin (mixed) boundary conditions are imposed, i.e.

$$x = 0, \qquad (z,t) \in \mathbb{R}^+ \times \partial\Omega_d \tag{3}$$

$$-\kappa \nabla x \cdot \boldsymbol{n} = hx, \qquad (z,t) \in \mathbb{R}^+ \times \partial\Omega_m \tag{4}$$

with $\partial\Omega = \partial\Omega_d \cup \partial\Omega_m$ the boundary of Ω. Here, $h(z)$ is the heat transfer coefficient and $(\kappa\nabla x) \cdot \boldsymbol{n}$ refers to the weighted derivative of $x(z,t)$ in the direction of the outer normal of the boundary surface $\partial\Omega$. The system is assumed to be initially in steady state

$$x = x_0 = \vartheta_0 - \vartheta_u, \quad z \in \overline{\Omega},\ t = 0, \tag{5}$$

where $x_0(z) = x^s(z)$ is a solution to

$$0 = \nabla \cdot (\kappa \nabla x^s) + \textstyle\sum_{j=1}^{m} b_j u_j^s,\ z \in \Omega \tag{6}$$

with the boundary conditions $x^s = 0$, $z \in \partial\Omega_d$ and $-\kappa \nabla x^s \cdot \boldsymbol{n} = hx^s$, $z \in \partial\Omega_m$, given constant input values $u_j^s = u_{j,0}^s$, $j = 1, \ldots, m$.

2.2 Finite element approximation

The weak form of (1)-(5) permits to deduce a finite element (FE) approximation depending on the chosen set of spatial ansatz functions. Let $\delta x(z) \in H_d^1(\Omega) = \{f(z) \in H^1(\Omega) \,|\, f(z) = 0,\ z \in \partial\Omega_d\}$ denote a test function. Multiplication of (1) with $\delta x(z)$ and integration over Ω taking into account the divergence theorem yields

$$\begin{aligned}&\textstyle\int_\Omega \rho c_p \partial_t x \delta x \mathrm{d}\Omega + \int_\Omega \kappa \nabla x \cdot \nabla \delta x \mathrm{d}\Omega \\ &\quad - \textstyle\int_{\partial\Omega} \delta x (\kappa \nabla x \cdot \boldsymbol{n}) \mathrm{d}\partial\Omega = \sum_{j=1}^{m} u_j(t) \int_\Omega b_j \delta x \mathrm{d}\Omega.\end{aligned}$$

With (3), (4) and $\delta x(z) = 0$ for $z \in \partial\Omega_d$ this expression simplifies to

$$\begin{aligned}&\textstyle\int_\Omega \rho c_p \partial_t x \delta x \mathrm{d}\Omega + \int_\Omega \kappa \nabla x \cdot \nabla \delta x \mathrm{d}\Omega \\ &\quad + \textstyle\int_{\partial\Omega_m} \delta x h x \mathrm{d}\partial\Omega_m = \sum_{j=1}^{m} u_j(t) \int_\Omega b_j \delta x \mathrm{d}\Omega\end{aligned} \tag{7}$$

for every test function $\delta x(z) \in H_d^1(\Omega)$. Let $\boldsymbol{e}(z) : \Omega_e \subset \Omega \to \mathbb{R}^n$ be the vector of element shape functions satisfying $\boldsymbol{e}(z) = \boldsymbol{0}$, $z \in \partial\Omega_d$ and let $\boldsymbol{q}_e(t) : \mathbb{R}^+ \to \mathbb{R}^n$ denote the nodal temperature vector of the element. Hence, the separation ansatz $x(z,t) = \boldsymbol{e}^T(z)\boldsymbol{q}_e(t)$ and $\delta x(z) = \boldsymbol{e}^T(z)\delta\boldsymbol{q}$ for arbitrary variations $\delta\boldsymbol{q}$ provides

$$\begin{aligned}\delta\boldsymbol{q}^T \Big\{ &\underbrace{\textstyle\int_\Omega \rho c_p \boldsymbol{e}\boldsymbol{e}^T \mathrm{d}\Omega}_{=:C_e} \partial_t \boldsymbol{q}_e - \underbrace{\textstyle\sum_{j=1}^{m} u_j(t) \int_\Omega b_j \boldsymbol{e} \mathrm{d}\Omega}_{=:B_e \boldsymbol{u}} \\ &+ \underbrace{\left(\textstyle\int_\Omega \kappa J_{\boldsymbol{e}} J_{\boldsymbol{e}}^T \mathrm{d}\Omega + \int_{\partial\Omega_m} h \boldsymbol{e}\boldsymbol{e}^T \mathrm{d}\partial\Omega_m\right)}_{=:K_e} \boldsymbol{q}_e(t) \Big\} = 0,\end{aligned}$$

where $J_{\boldsymbol{e}}(z) = \partial_z \boldsymbol{e}(z)$ denotes the Jacobian matrix. Since the latter equation has to hold for any variation $\delta\boldsymbol{q}$ the equations for a single element follow as $C_e \partial_t \boldsymbol{q}_e + K_e \boldsymbol{q}_e = B_e \boldsymbol{u}$. Taking into account the connectivity information and eliminating the nodal constraints including the Dirichlet condition, (3) permits to assemble the global equations in the form

$$C \partial_t \boldsymbol{q} + K \boldsymbol{q} = B \boldsymbol{u}. \tag{8}$$

Here, $\boldsymbol{q}(t) \in \mathbb{R}^n$ summarizes nodal temperatures, $C \in \mathbb{R}^{n \times n}$ is the thermal damping or thermal capacity matrix, $K \in \mathbb{R}^{n \times n}$ denotes the heat transfer matrix,

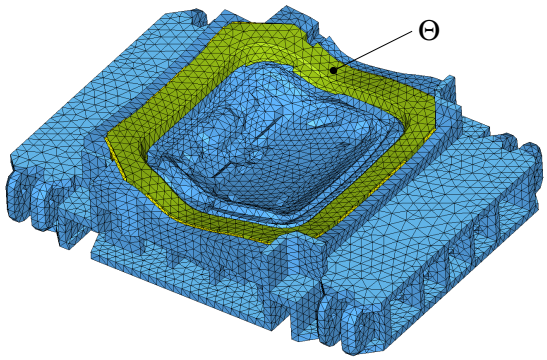

Fig. 2. FE mesh of the die with about 20.000 nodes. Part Θ of the blankholder area describes the target variables.

$B \in \mathbb{R}^{n\times m}$ represents the input matrix, and $\boldsymbol{u}(t) = [u_1(t),\dots,u_m(t)]^T \in \mathbb{R}^m$ is the input vector. The initial condition $x_0(z)$ by assumption corresponds to a steady state solution which translates into $\boldsymbol{q}(0) = \boldsymbol{q}_0^s$ with $\boldsymbol{q}_0^s$ satisfying

$$K\boldsymbol{q}^s = B\boldsymbol{u}^s \tag{9}$$

for $\boldsymbol{u}^s = \boldsymbol{u}_0^s = [u_{1,0}^s,\dots,u_{m,0}^s]^T$.

In this setting, trajectory planning for the deep drawing tool refers to the determination of the input trajectory $t \mapsto \boldsymbol{u}^*(t)$ to realize the transition from the initial (stationary) temperature profile $\boldsymbol{q}(0) = \boldsymbol{q}_0^s$ to a desired final (stationary) temperature profile $\boldsymbol{q}(T) = \boldsymbol{q}_T^s$ within a prescribed finite time interval $t \in [0,T]$ along a predefined transition path $\boldsymbol{q}^*(t)$. In particular, a desired transient temperature profile is requested for a subpart Θ in the blankholder area shown in Fig. 2. These target variables are subsequently summarized in the vector

$$\boldsymbol{y}_{\text{targ}} = H_{\text{targ}}\boldsymbol{q} \tag{10}$$

with the matrix $H_{\text{targ}} \in \mathbb{R}^{p\times n}$ extracting the respective nodal temperatures from $\boldsymbol{q}(t)$. For the mesh of Fig. 2 p is 362. Temperature measurements are available at 12 locations inside the die, i.e.

$$\boldsymbol{y} = H_{\text{meas}}\boldsymbol{q} \tag{11}$$

with $H_{\text{meas}} \in \mathbb{R}^{12\times n}$. These are used for the feedback control design and to validate the control performance.

3. FLATNESS-BASED TRAJECTORY PLANNING

Modal or spectral analysis serves as the basis for the determination of a flatness-based state and input parametrization for the FE approximation (8) with (10) and (11). With this, a particularly intuitive solution to the trajectory planning problem is obtained.

3.1 Spectral system representation

Let V denote the matrix of eigenvectors $\{\boldsymbol{v}_k\}_{k=1,\dots,n}$ arsing from the solution of the generalized eigenproblem $CV = -KV\Lambda$ with $\Lambda = \operatorname{diag}\{\lambda_k\}_{k=1}^n$ the diagonal matrix of eigenvalues λ_k. Then the similarity transformation $\boldsymbol{q}(t) = V\boldsymbol{\eta}(t)$ applied to (8) results in the modal or spectral system representation

$$\partial_t\boldsymbol{\eta} = \Lambda\boldsymbol{\eta} + \Upsilon\boldsymbol{u} \tag{12}$$

with $\Upsilon = (CV)^{-1}B$. Herein it is assumed that the eigenvalues are mutually disjoint. This assumption is supported by numerical results. For the general situation of eigenvalues with algebraic multiplicity larger than one, the reader is referred to Meurer [2013].

3.2 Differential state and input parametrization

Application of the Laplace transform to (12) yields

$$\begin{aligned}\hat{\boldsymbol{\eta}} &= (sI-\Lambda)^{-1}\Upsilon\hat{\boldsymbol{u}}(s)\\ &= -\big(I - s\Lambda^{-1}\big)^{-1}\Lambda^{-1}\Upsilon\hat{\boldsymbol{u}} = -\frac{D^x(s)}{D^u(s)}\Lambda^{-1}\Upsilon\hat{\boldsymbol{u}}\end{aligned}$$

Herein, s is the Laplace operator, I is the $n\times n$ identity matrix and $\hat{\cdot}$ refers to the Laplace transformed variables. Recalling that Λ is a diagonal matrix with disjoint entries, the terms $D^x(s)$ and $D^u(s)$ can be reformulated to obtain

$$D^x(s) = \operatorname{adj}(I - s\Lambda^{-1}) = \operatorname{diag}\left\{\prod_{\substack{j=1\\ j\neq k}}^{n}\left(1-\frac{s}{\lambda_j}\right)\right\}_{k=1}^{n} \tag{13}$$

$$D^u(s) = \det(I - s\Lambda^{-1}) = \prod_{j=1}^{n}\left(1-\frac{s}{\lambda_j}\right), \tag{14}$$

where $\operatorname{adj}(\cdot)$ refers to the adjugate matrix. The introduction of the new variable $\hat{\boldsymbol{\zeta}}(s) = \hat{\boldsymbol{u}}(s)/D^u(s)$ provides a parametrization of states and inputs in the operational domain according to

$$\hat{\boldsymbol{\eta}} = -D^x(s)\Lambda^{-1}\Upsilon\hat{\boldsymbol{\zeta}}, \quad \hat{\boldsymbol{u}} = D^u(s)\hat{\boldsymbol{\zeta}}.$$

The corresponding expressions in the time domain follow by taking into account that s is equivalent to time differentiation, which implies

$$\boldsymbol{\eta} = -D^x(\partial_t)\circ\Lambda^{-1}\Upsilon\boldsymbol{\zeta} \tag{15a}$$

$$\boldsymbol{u} = D^u(\partial_t)\circ\boldsymbol{\zeta} \tag{15b}$$

with $D^x(\partial_t)$ and $D^u(\partial_t)$ being interpreted as differential operators of order $n-1$ or n, respectively. Thus, $\boldsymbol{\zeta}(t)$ can be called a flat or basic output differentially parametrizing state and input. Similarly, the parametrization of the target variables (10) is given by

$$\boldsymbol{y}_{\text{targ}} = H_{\text{targ}}V\boldsymbol{\eta} = -H_{\text{targ}}VD^x(\partial_t)\circ\Lambda^{-1}\Upsilon\boldsymbol{\zeta}. \tag{15c}$$

It is obvious that any desired trajectory $t \mapsto \boldsymbol{\zeta}^*(t)$ for the flat output has to be at least n-times continuously differentiable. With this, the feedforward control $\boldsymbol{u}^*(t)$ which is necessary to realize $\boldsymbol{\eta}^*(t)$ determined in (15a) and equivalently $\boldsymbol{y}_{\text{targ}}^*(t)$ from (15c) follows directly from the evaluation of (15b) for $\boldsymbol{\zeta}(t)$ replaced by $\boldsymbol{\zeta}^*(t)$.

3.3 Trajectory assignment

The stationary temperature $\boldsymbol{q}^s$ of the die is determined from (9), i.e., $K\boldsymbol{q}^s = B\boldsymbol{u}^s$ for constant input $\boldsymbol{u}^s$. Now let $\boldsymbol{q}_0^s$ and $\boldsymbol{q}_T^s$ denote the initial and the desired final stationary temperature profile. Taking into account the input parametrization (15b) with $D^u(s)$ from (14) under steady state conditions, i.e. $\boldsymbol{u}^s = \boldsymbol{\zeta}^s$, an alternative formulation of the steady state equations is given by $K\boldsymbol{q}^s = B\boldsymbol{\zeta}^s$ such that

$$K\boldsymbol{q}_T^s = B\boldsymbol{\zeta}_T^s. \tag{16}$$

Since $\dim\boldsymbol{q}_T^s = n$ and $\dim\boldsymbol{\zeta}_T^s = \dim\boldsymbol{u} = m \ll n$ is given, $\boldsymbol{q}_T^s$ a solution to (16) cannot be obtained exactly but as the solution to a least-squares minimization problem $\min_{\boldsymbol{\zeta}_T^s}\frac{1}{2}\|K\boldsymbol{q}_T^s - B\boldsymbol{\zeta}_T^s\|_2^2$ subject to $\boldsymbol{\zeta}_T^s \in [0,\bar{u}]$. This

formulation can be extended by taking into account the weighted heat flux, subsequently referred to as $\nabla \boldsymbol{q}_T^s$, to limit temperature gradients inside the tool, i.e.

$$\begin{aligned} \min_{\boldsymbol{\zeta}_T^s} & \big(a_0 \|K\boldsymbol{q}_T^s - B\boldsymbol{\zeta}_T^s\|_2^2 + \|\boldsymbol{a}_1 \cdot \nabla \boldsymbol{q}_T^s\|_2^2\big) \\ \text{s.t.} \quad & \boldsymbol{\zeta}_T^s \in [0, \bar{u}]. \end{aligned} \tag{17}$$

Thereby, a_0 and $\boldsymbol{a}_1 = [a_{11}, a_{12}, a_{13}]^T$ denote weighting factors.

In view of (15c) it follows in steady state that $\boldsymbol{y}_{\text{targ}}^s = -H_{\text{targ}} V \Lambda^{-1} \Upsilon \boldsymbol{\zeta}^s$. Hence, instead of prescribing a steady state temperature profile for the whole die it is reasonable to prescribe desired final temperatures $\boldsymbol{y}_{\text{targ,T}}^s$ for the target variables only. In this case, (17) can rewritten as

$$\begin{aligned} \min_{\boldsymbol{\zeta}_T^s} & \big(a_0 \|\boldsymbol{y}_{\text{targ,T}}^s + H_{\text{targ}} V \Lambda^{-1} \Upsilon \boldsymbol{\zeta}_T^s\|_2^2 + \|\boldsymbol{a}_1 \cdot \nabla \boldsymbol{y}_{\text{targ,T}}^s\|_2^2\big) \\ \text{s.t.} \quad & \boldsymbol{\zeta}_T^s \in [0, \bar{u}] \end{aligned} \tag{18}$$

with $\nabla \boldsymbol{y}_{\text{targ,T}}^s$ referring to the corresponding heat flux. It is obvious that optimization criteria differing from (18) can be defined to compute $\boldsymbol{\zeta}_T^s$ i.e. depending on the considered task.

Numerical results are shown in Fig. 3(a), presenting the approximation $\bar{\boldsymbol{y}}_{\text{targ,T}}^s = -H_{\text{targ}} V \Lambda^{-1} \Upsilon \boldsymbol{\zeta}_T^s$ according to (18) of the desired temperature profile $\boldsymbol{y}_{\text{targ,T}}^s = 35 \times \mathbf{1}$ at the blankholder with the unit vector $\mathbf{1}$ and the coefficients $a_0 = 12$, $\boldsymbol{a}_1 = [1.75, 1.75, 0]^T$ for a specific heating cartridge configuration.

Once $\boldsymbol{\zeta}_T^s$ is computed, a desired path $\boldsymbol{\zeta}^*(t)$ for the flat output $\boldsymbol{\zeta}(t)$ has to be determined connecting the initial and the desired final steady state. For this, consider

$$\boldsymbol{\zeta}^* = \boldsymbol{\zeta}_0^s + (\boldsymbol{\zeta}_T^s - \boldsymbol{\zeta}_0^s)\Phi \tag{19}$$

with the function $\Phi_T(t) \in C^n(\mathbb{R})$ satisfying $\Phi(t \leq 0) = 0$, $\Phi(t \geq T) = 1$ and $\partial_t^j \Phi(t) = 0$, $j \geq 1$ for $t \in \{0, T\}$. Typically smooth but locally non-analytic Gevrey-class functions are imposed for $\Phi(t)$. For further details and particular functions $\Phi(t)$ the reader is referred to Fliess et al. [1997], Lynch and Rudolph [2002], Meurer [2013].

3.4 Convergence in the continuous limit and divergent parametrizations

Convergence of the parametrizations (15) crucially depends on the distribution of the eigenvalues λ_k, $k = 1, \ldots, n$. For the convergence analysis the entire function theory can be utilized in order to address the continuous limit as $n \to \infty$, i.e. when the FE approximation approaches the distributed-parameter system description. In this case, both $D^x(s)$ and $D^u(s)$ have to be interpreted as Hadamard factorizations of entire functions in the complex domain $s \in \mathbb{C}$. The analysis makes use of the so-called counting function $\mathfrak{n}(r) = \#\{\lambda_k,\, k \in \mathbb{N} : |\lambda_k| \leq r\}$ of the sequence of eigenvalues $(\lambda_k)_{k \in \mathbb{N}}$ with $\#$ referring to the number of elements in the set. Taking into account the Weyl asymptotic formula for the eigenvalues of the heat equation allows to deduce an asymptotic expression for the growth property of $\mathfrak{n}(r)$ in the coefficient r. The remaining analysis then relies on the utilization of these results for the determination of the order of growth and type of the entire function $D^u(s)$ and can be found in Meurer [2013].

In particular, it can be shown for the 3D heat equation with finite-dimensional in-domain actuation that convergence of the parametrizations (15) cannot be guaranteed in general in the continuous limit. This is, however, a rather common outcome in DPS control and has already been analyzed, e.g., for the boundary controlled linear wave equation [Rouchon, 2005] or diffusion-reaction systems [Meurer, 2011].

Nevertheless, the divergent behavior does not limit the applicability of the presented flatness-based trajectory planning approach. To address this, suitable re-summation techniques are integrated into the design which accelerate convergence and even allow to determine a meaningful limit from the divergent parametrizations. For this, observe that (15b) admits a polynomial representation in the form

$$\boldsymbol{u} = \sum_{j=0}^{n} p_j \partial_t^j \boldsymbol{\zeta}, \quad p_0 = 1. \tag{20}$$

In the subsequent simulation and experimental results the so-called (N, ξ)-approximate k-summation $\mathcal{S}_k^{N,\xi}$ is used to determine the feedforward control by evaluating

$$\boldsymbol{u} \mapsto \big(S_k^{N,\xi} \boldsymbol{u}\big) = \frac{\sum_{j=0}^{N} \boldsymbol{s}_j \frac{\xi^j}{\Gamma(1+j/k)}}{\sum_{j=0}^{N} \frac{\xi^j}{\Gamma(1+j/k)}}. \tag{21}$$

Herein, $\boldsymbol{s}_j(t) = \sum_{i=0}^{j} p_i \partial_t^i \boldsymbol{\zeta}(t)$ is the partial sum and $N \in \mathbb{N}$, $N \leq n$. The parameters ξ and k in $\mathcal{S}_k^{N,\xi}$ can be considered as degrees-of-freedom which have to be appropriately determined depending on the behavior of the coefficients in (20). A similar setting can be introduced to evaluate the state parametrization (15a) and hence $\boldsymbol{q}(t) = V\boldsymbol{\eta}(t)$. For further details the reader is referred to Meurer and Zeitz [2005].

4. RESULTS

In the following, simulation and measurement results are provided which underline the applicability of the proposed design technique for the deep drawing tool. The transition time is assigned as $T = 7200\,\text{s}$, motivated by the practial implementation where the start of production is timed and the duration of the pre-heating is limited by the set-up time of the tool. The die is equipped with $m = 18$ heating cartridges. The ambient temperature for simulation and measurement is approx. $\vartheta_u = 25\,^\circ\text{C}$ and equals the initial temperature $\vartheta_0(z)$ of the tool. The target temperature for $\boldsymbol{y}_{\text{targ}}(t)$ defined in (10) is $35\,^\circ\text{C}$. The desired trajectory $\boldsymbol{\zeta}^*(t)$ for the flat output $\boldsymbol{\zeta}(t)$ is assigned using (19) for $\boldsymbol{\zeta}_0^s = \mathbf{0}$ (since $\vartheta_u = \vartheta_0$) and $\boldsymbol{\zeta}_T^s$ determined by solving (18). The control performance is evaluated by considering the measured temperatures (11) and their deviation from the reference $\boldsymbol{y}^*(t) = H_{\text{meas}} \boldsymbol{q}^*(t) = H_{\text{meas}} V \boldsymbol{\eta}^*(t)$. The die consists of cast material EN-JS 2070. The armor ring is made of wear-resistant cast iron 1.2382. The material parameters and contact conditions are gathered from literature.

4.1 Simulation results

Simulation results for feedforward control $\boldsymbol{u}^*(t) \in [0, \bar{u}]$ obtained from the evaluation of (21) with $\boldsymbol{\zeta}^*(t)$ from (19)

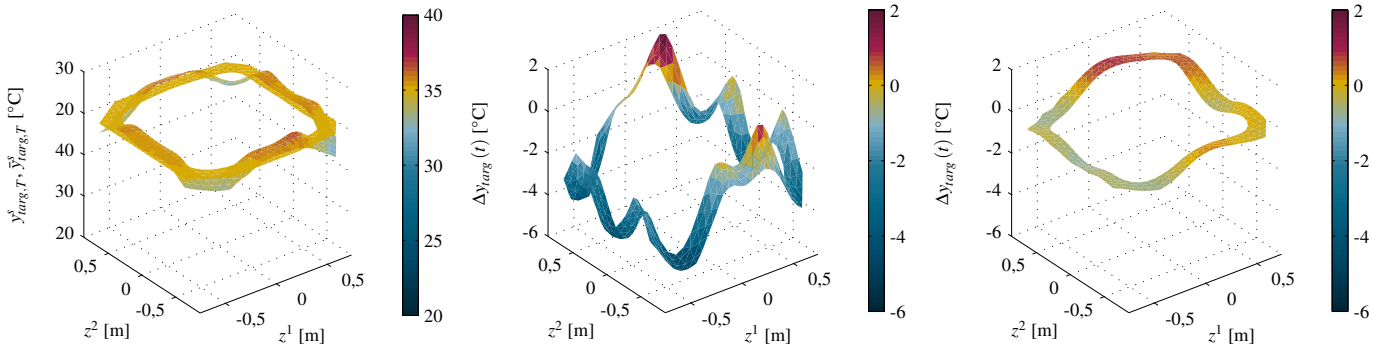

(a) Comparison of target profile $\boldsymbol{y}^s_{\mathrm{targ,T}} = 35 \times \mathbf{1}$ and approximation $\bar{\boldsymbol{y}}^s_{\mathrm{targ,T}}$ using (18).

(b) Error $\Delta \boldsymbol{y}_{\mathrm{targ}}(t) = \boldsymbol{y}_{\mathrm{targ}}(t) - \bar{\boldsymbol{y}}^s_{\mathrm{targ,T}}$ for $t = 7200\,\mathrm{s}$ (simulation).

(c) Error $\Delta \boldsymbol{y}_{\mathrm{targ}}(t) = \boldsymbol{y}_{\mathrm{targ}}(t) - \bar{\boldsymbol{y}}^s_{\mathrm{targ,T}}$ for $t = 14400\,\mathrm{s}$ (simulation).

Fig. 3. Temperature profiles and temperature evolution for the blankholder area Θ (cf. also Fig. 2).

are shown in Fig. 5(a). Since flatness does not allow to explicitly take into account input constraints, the input trajectory is cut-off whenever $\boldsymbol{u}^*(t)$ is outside the interval $[0, \bar{u}]$ with $\bar{u} = 0.8 u_{\max}$. The utilization of only 80% of the maximal heating power of the cartridges is motivated by the practical implementation, where an additional output error feedback controller is added to the feedforward control. Here, the simulated time evolution of the output variables y_i, the tracking error $\Delta y_i = y_i - y_i^* = 0$ and the applied open-loop input trajectory $\boldsymbol{u}^*(t)$ are depicted.

As expected and illustrated in Fig. 3(b), the cut-off results in a delayed convergence to the desired final steady state profile. However, Fig. 3(c) showing the temperature profile at twice the prescribed transition time $t = 14400\,\mathrm{s}$ confirms the homogenization of the temperature evolution in the blankholder area Θ (cf. Fig. 2) to the desired temperature level.

4.2 Measurement results

The controller implementation is PC-based including a commercial MIMO PID heating controller. The PC and the controller are connected by an `RS485` interface using the protocol of the heating controller. The heating controller is only used to adjust the output power. The temperatures in the blankholder area are measured with commercial temperature sensors. The feedforward and the subsequently addressed feedback controller are realized using `LabView` including `Mathscript`. The sampling time is $T_s = 60\,\mathrm{s}$.

Measurement results for the pure feedforward control $\boldsymbol{u}^*(t)$ according to (21) with $\boldsymbol{\zeta}^*(t)$ from (19) are shown in Fig. 5(b). As can be seen, rather accurate temperature tracking is achieved. However, model uncertainties (especially the heat transfer between tool and heating cartridges) and disturbances lead to a steady state error, motivating the combination of the feedforward part with a suitable output error feedback control.

For the feedback part a decentralized PID controller is used in a two-degrees-of-freedom (2DOF) control structure according Fig. 4. In this set-up, the setpoint change and the desired trajectory are realized by the feedforward controller $\boldsymbol{u}^*(t)$ while the feedback controller $\Delta \boldsymbol{u}(t)$ only stabilizes the tracking error. The coupling of the outputs

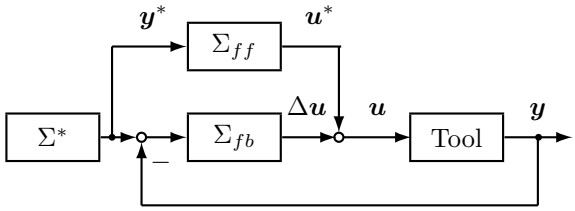

Fig. 4. Block diagram of the two-degree-of-freedom control scheme for the deep drawing tool with feedforward control Σ_{ff}, feedback control Σ_{fb}, and trajectory generator Σ^* for output tracking $\boldsymbol{y}(t) \to \boldsymbol{y}^*(t)$ or $\boldsymbol{y}_{\mathrm{targ}}(t) \to \boldsymbol{y}^*_{\mathrm{targ}}(t)$, respectively.

and inputs for the decentralized MIMO control design is addressed by the stationary relative gain array (RGA) analysis to properly relate the 12 temperature sensors and the 18 heating cartridges by individual PID controllers. The parameters of the PID control are determined using the H_∞-loop-shaping method by Glover-MacFarlane to achieve robust performance.

Measurement results for the flatness-based two-degree-of-freedom control are depicted in Fig. 5(c). Obviously, the arising deviations are reduced by the feedback part so that accurate tracking can be achieved for the deep drawing tool. Moreover, the characteristic behavior of the 2DOF control concept becomes visible, where, as pointed out above, the desired path is mainly realized by the feedforward term with the feedback part addressing only the tracking error. When comparing the two lower pictures in Figs. 5(b) and 5(c), only minor distortions of the control signal emerge due to the feedback controller.

5. CONCLUSIONS

In this contribution, a flatness-based approach for trajectory planning for a deep drawing tool is presented to realize setpoint changes and desired temperature trajectories. A finite element approximation of the governing heat equation is considered to address the complex tool geometry. Based on the finite-dimensional approximation, a spectral design technique is developed, solely making use of the eigenvalues and eigenvectors of the system matrices. With this, a flat output parameterizing system states, inputs and outputs is systematically con-

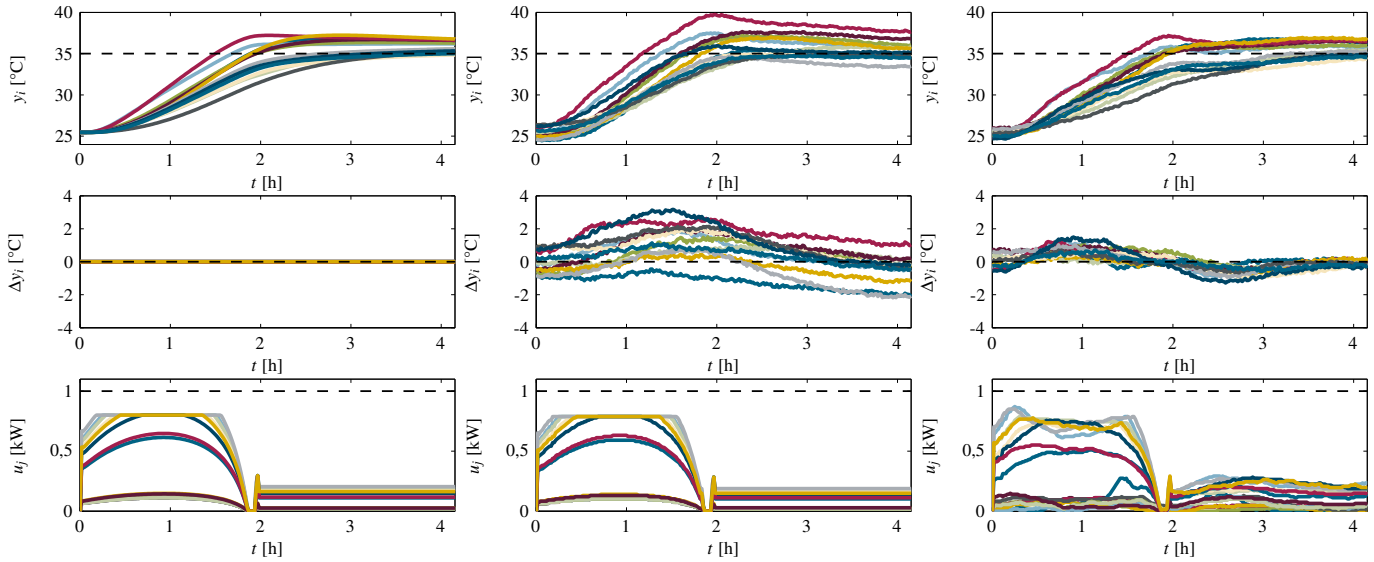

(a) Feedforward control (simulation). (b) Feedforward control (measurement). (c) 2DOF control (measurement).

Fig. 5. Simulation and measurement results for feedforward control and its combination with decentralized PID-control with a two-degrees-of-freedom (2DOF) control approach.

structed. To achieve the desired spatial-temporal temperature paths, suitable trajectory assignment is addressed in terms of a minimization problem to determine the final value of the flat output depending on the prescribed temperature level in the tool interior. The convergence analysis in the limit as the finite element approximation approaches the distributed-parameter system reveals that the flatness-based parametrizations may diverge in general. To overcome this appropriate re-summation technique are integrated into the design. Simulation and measurement results confirm the applicability of the design approach and illustrate the tracking performance which can be obtained by applying only the feedforward controller as well as by considering a 2DOF approach combining feedforward and output error feedback control. With this, a first experimental validation of flatness-based trajectory planning for distributed-parameter thermal systems with 3-dimensional domain and in-domain actuation is achieved.

Ongoing research addresses the reconstruction of the unmeasured temperatures in the tool from the available measurements as well as suitable techniques for the optimal actuator and sensor placement. Moreover, the presented feedforward control design shows great potential for partial or variothermal heating in warm deep drawing to increase the accuracy and velocity of the heating processes. Empirical testing is needed for a successful implementation in these areas.

REFERENCES

T. Böhm, R. Struck, A. Matveev, T. Meurer, and M. Dagen. Model Based Feedforward Temperature Reference Control of a Deep Drawing Tool. In *IDDRG Conference Proceedings*, pages 41–46, Zürich, Schweiz, Juni 2013.

R.F. Curtain and H.J. Zwart. *An Introduction to Infinite–Dimensional Linear Systems Theory*. Springer–Verlag, New York, 1995.

M. Fliess, J. Lévine, P. Martin, and P. Rouchon. Flatness and Defect of Non–Linear Systems: Introductory Theory and Examples. *Int. J. Control*, 61:1327–1361, 1995.

M. Fliess, H. Mounier, P. Rouchon, and J. Rudolph. Systèmes linéaires sur les opérateurs de Mikusiński et commande d'une poutre flexible. *ESAIM Proceedings*, 2:183–193, 1997.

B. Laroche, P. Martin, and P. Rouchon. Motion Planning for the Heat Equation. *Int. J. Robust Nonlinear Control*, 10:629–643, 2000.

A.F. Lynch and J. Rudolph. Flatness–based Boundary Control of a Class of Quasilinear Parabolic Distributed Parameter Systems. *Int. J. Control*, 75(15):1219–1230, 2002.

T. Meurer. Flatness–based Trajectory Planning for Diffusion–Reaction Systems in a Parallelepipedon — A Spectral Approach. *Automatica*, 47(5):935–949, 2011.

T. Meurer. *Control of Higher–Dimensional PDEs: Flatness and Backstepping Designs*. Communications and Control Engineering Series. Springer–Verlag, 2013.

T. Meurer and A. Kugi. Trajectory Planning for Boundary Controlled Parabolic PDEs with Varying Parameters on Higher-dimensional Spatial Domains. *IEEE T. Automat. Contr.*, 54(8):1854–1868, 2009.

T. Meurer and M. Zeitz. Feedforward and Feedback Tracking Control of Nonlinear Diffusion–Convection–Reaction Systems Uusing Summability Methods. *Ind. Eng. Chem. Res.*, 44:2532–2548, 2005.

N. Petit and P. Rouchon. Flatness of Heavy Chain Systems. *SIAM J. Control Optim.*, 40(2):475–495, 2001.

N. Petit and P. Rouchon. Dynamics and Solutions to Some Control Problems for Water-tank Systems. *IEEE Trans. Automatic Control*, 47(4):594–609, 2002.

P. Rouchon. Flatness–based Control of Oscillators. *Z. Angew. Math. Mech.*, 85(6):411–421, 2005.

J. Rudolph. *Flatness Based Control of Distributed Parameter Systems*. Berichte aus der Steuerungs– und Regelungstechnik. Shaker–Verlag, Aachen, 2003.